Journal of *Marine Science and Engineering*

MDPI

Article

Static Design for Laterally Loaded Rigid Monopiles in Cohesive Soil

Ruping Luo [1,2], Mingluqiu Hu [1], Min Yang [3], Weichao Li [3,*] and Anhui Wang [4]

[1] School of Civil Engineering and Architecture, East China Jiaotong University, Nanchang 330013, China
[2] Key Laboratory of Ministry of Education for Geomechanics and Embankment Engineering, Hohai University, Nanjing 210098, China
[3] Department of Geotechnical Engineering, Tongji University, 1239 Siping Road, Shanghai 200092, China
[4] China Construction Industrial & Energy Engineering Group Co., Ltd., Nanjing 210023, China
* Correspondence: weichaoli@tongji.edu.cn; Tel.: +86-21-65983386

Abstract: Rigid monopiles with small slenderness ratios (i.e., ratio of monopile embedded length to outer diameter) are widely used as foundations to resist lateral load and moment transferred from superstructures, e.g., large diameter steel pipes used by offshore wind turbines and piers in electric utility industry or sound barriers. A design model for laterally loaded rigid monopiles in cohesive soil is presented in this paper. The proposed design model assumes a constant depth of rotation point as well as a trilinear distribution model of soil lateral reaction along the embedded length of the monopile, and introduces a mobilization coefficient of soil reaction to quantify the magnitude of soil reaction mobilized under a certain load applied at the monopile head. The relationship between the mobilization coefficient and monopile head rotation is established by back-analyzing test results measured from series of laterally loaded pile tests, and then a general design procedure for a laterally loaded rigid monopile in cohesive soil is recommended. The feasibility and reliability of the proposed design model is validated against three cases of numerical simulations on laterally loaded piles in cohesive soils. It shows that this study's proposed design model produces a relatively satisfactory prediction of the nonlinear load-deformation response, and can be used for laterally loaded monopile design in the sites with undrained shear strength being uniform or increasing linearly with depth.

Keywords: monopiles; rotation depth; lateral load; cohesive soils; design method

check for updates

Citation: Luo, R.; Hu, M.; Yang, M.; Li, W.; Wang, A. Static Design for Laterally Loaded Rigid Monopiles in Cohesive Soil. *J. Mar. Sci. Eng.* **2023**, *11*, 817. https://doi.org/10.3390/jmse11040817

Received: 2 March 2023
Revised: 30 March 2023
Accepted: 1 April 2023
Published: 12 April 2023

Copyright: © 2023 by the authors. Licensee MDPI, Basel, Switzerland. This article is an open access article distributed under the terms and conditions of the Creative Commons Attribution (CC BY) license (https://creativecommons.org/licenses/by/4.0/).

1. Introduction

Rigid monopiles with small slenderness ratios (i.e., ratio of pile embedded length to outer diameter) have been widely used for supporting lateral or axial loads for various structures, e.g., transmission lines and offshore wind turbines (OWTs) [1,2]. This is especially true for the monopiles used for supporting OWTs, accounting for more than 80% of currently installed OWTs [3]. Differing from the piles used in the traditional offshore oil and gas industry (with relatively small diameters D less than 2.5 m), the diameters of the piles used in offshore wind industry are usually in the range between 4 and 6 m [4], which can be regarded as large diameter monopiles [5,6].

For the offshore wind turbines, winds- and waves-induced lateral loads generally govern the design of monopile, and the lateral displacement or rotation are more concerned in the engineering foundation design. Over the years, a series of methods have been developed to predict the load-displacement response of laterally loaded piles. Since the 1970's, the Winkler-foundation-based P-y method, e.g., Matlock [7], Reese et al. [8] and Kim et al. [9], is developed extensively and is recommended by some design guidelines for piles generally used for the offshore oil and gas sector. Even though this method gives successful design for the laterally loaded long flexible piles, the applicability and reliability of this method is questioned by many researchers when being applied to the design of larger diameter rigid monopile with slenderness ratios generally smaller than 10 [10–12].

Munaga and Gonavaram [13] conducted a series of laboratory model tests to investigate the behavior of individual pile and pile groups under lateral loads in uniform sand and stratified soil (sand overlain by clay), the model test results show that the pile head deflection of the single pile and pile group was reduced for the stratified soil when compared to the uniform sand bed. Rathod et al. [14] examined the effects of embedded length and the asymmetric two-way cyclic loads on the lateral pile head displacements via a series of 1 g model tests. In order to investigate the effects of anisotropy of sand on a cyclic laterally loaded monopile, Yu et al. [15] conducted a series of 1 g model tests. It was found that for a monopile in sandy soil, the accumulated displacements at the pile head increased with the increased deposition angles of sand. Kozubal et al. [16] conducted a series of three-dimensional numerical models to analyzing laterally loaded piles, and a pronounced effect of the random variability of both the lateral force and the elastic modulus of the upper layer on reliability indices has been observed. Based on the numerical models, Li et al. [17] investigate the laterally loaded behavior of hybrid monopiles in the locally scoured sandy seabed, and the effects of the relative density of sand is discussed. A series of well-calibrated finite-element (FE) analyses using an advanced state-dependent constitutive model are conducted by Wang et al. [18] to study the influence of pile diameter and aspect ratio on the lateral bearing behavior of monopiles, and a simple design model was proposed to calculate the combined capacity of rigid piles based on the observed pile–soil interaction mechanism. Huchegowda et al. [19] determined the lateral load capacity using the finite element method (FEM) for pile in layered soil, and the results obtained from the study indicated that the lateral capacity of pile foundation depends on the cross-sectional area and material of the pile, boundary conditions of the pile at top and bottom, and horizontal subgrade modulus of top soil (6D, where D is diameter of pile).

In addition to the numerical simulations and model tests, in order to predict the load-displacement response of laterally loaded rigid monopile, analytical methods based on the force and moment equilibriums solutions are proposed by Zhang [20], Motta [21], Zhang and Ahmari [22], and Fu et al. [23]. For example, Zhang [20] assumed that both the ultimate soil resistance and the modulus of horizontal subgrade reaction increase linearly with depth. By considering the force and moment equilibrium, the system equations are derived for a rigid pile under a lateral eccentric load. In general, these analytical approaches are derived based on the rigid pile assumption, in which the laterally loaded piles are considered to undergo rigid body rotation, and the distribution models of soil reaction and horizontal subgrade reaction modulus are assumed. It should be noted that, however, in order to obtain a good prediction of rigid monopile response, the modulus of horizontal subgrade reaction should be carefully examined, and an iteration program is needed to solve the high order nonlinear equations [20].

In this study, a static design with the nonlinear analysis of laterally loaded rigid monopiles in cohesive soil is developed. Compared to the methods proposed by Zhang [20], Motta [21], and Zhang and Ahmari [22], one obvious advantage of this method is that it can be employed without computer programing, and the input parameters can be conveniently obtained through conventional laboratory or field tests in practical design. In this method, the lateral soil reaction is assumed to vary in a trilinear pattern with depth, and a soil reaction mobilization coefficient is introduced to evaluate the mobilization of lateral soil resistance with monopile rotation. The correlation between mobilization coefficient and monopile rotation is back-analyzed on measured results from a series of test piles. The general design procedure for a laterally loaded rigid monopile in cohesive soil is recommended, which is verified against three numerical cases. Comparison of pile response shows that this study-proposed design produces a reasonably good prediction for monopiles in cohesive soil.

2. Proposed Design Model

2.1. Depth of Rotation Point

Figure 1 shows a monopile with embedded length of L_{em} and outer diameter of D, under lateral load F at a height of L_{up}. If the relative stiffness ($\frac{L_{em}}{\sqrt[5]{E_p I_p / n_h}}$) between ground soil and monopile is smaller than 2 [24], the monopile under lateral loading rotates as a rigid body around a point located at some depth below the ground surface.

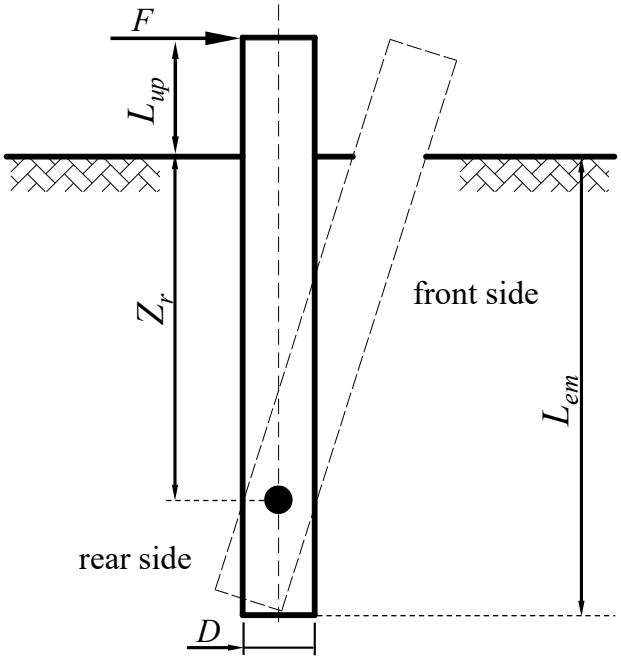


Figure 1. Sketch of a rigid monopile under lateral load.

In order to investigate the depth and the variation of the rotation point, a series of pile loading tests are collected. These test piles have a wide range of pile dimensions, were loaded with various load eccentricities, and installed in clayey ground from soft to stiff. The details of these pile tests are summarized in Table 1. The variation of L_{up} is from $0.2D$ to $7.89D$ for the pile loading tests collected in this paper. As concluded by Klinkvort et al. [25], the general pile–soil interaction is not related to the eccentricity, and no "correct" load eccentricity exists for monopile testing. From this perspective, the load eccentricity of the pile loading tests collected in this paper are applicable for the analysis of monopile under lateral loads.

Table 1. Pile tests for determination of rotation point.

Pile No.	Field/Lab	Soil Condition	Prototype Pile Dimensions			Pile Type	Site Location	Reference
			D(m)	L_{em}/D	L_{up}/D			
PR1	Field	Stiff clay	0.92	6.6	0.83	Concrete pile	Texas A&M University	Kasch et al. [26]
PR2	Field	Stiff clay	0.92	5	0.87	Concrete pile	Texas A&M University	Holloway et al. [27]
PR3	Field	Firm to stiff clay	1.5	7.7	0	Concrete pile	Ontario, USA	Ismael & Klym [28]
PR4	Field	Stiff clay	0.92	5	0.87	Concrete pile	Texas A&M University	Bierschwale et al. [29]
PR5	Field	residual clay	0.45	4.4	1.78	Timber–concrete pile	Auckland, New Zealand	Pender and Rodgers [30]

Table 1. *Cont.*

Pile No.	Field/Lab	Soil Condition	Prototype Pile Dimensions			Pile Type	Site Location	Reference
			D(m)	L_{em}/D	L_{up}/D			
PR6~PR8	Field	soft clay	3.80	5.26	7.89	Aluminium pipe pile	University of Cambridge	Lau et al. [31]
PR9	Lab	Mexico Gulf clay	0.10	8	5	Aluminium pipe pile	University of Texas at Austin	Senanayake [32]

The variation of normalized rotation depth Z_r/L_{em} with normalized load F/F_u are presented in Figure 2, in which F is the applied lateral load and F_u is the ultimate load capacity of lateral loaded monopiles. For the case in which the ultimate load capacity of the test pile was not specified in the literature, the ultimate load capacity was taken as the load at a pile-head displacement of 0.1D [33].

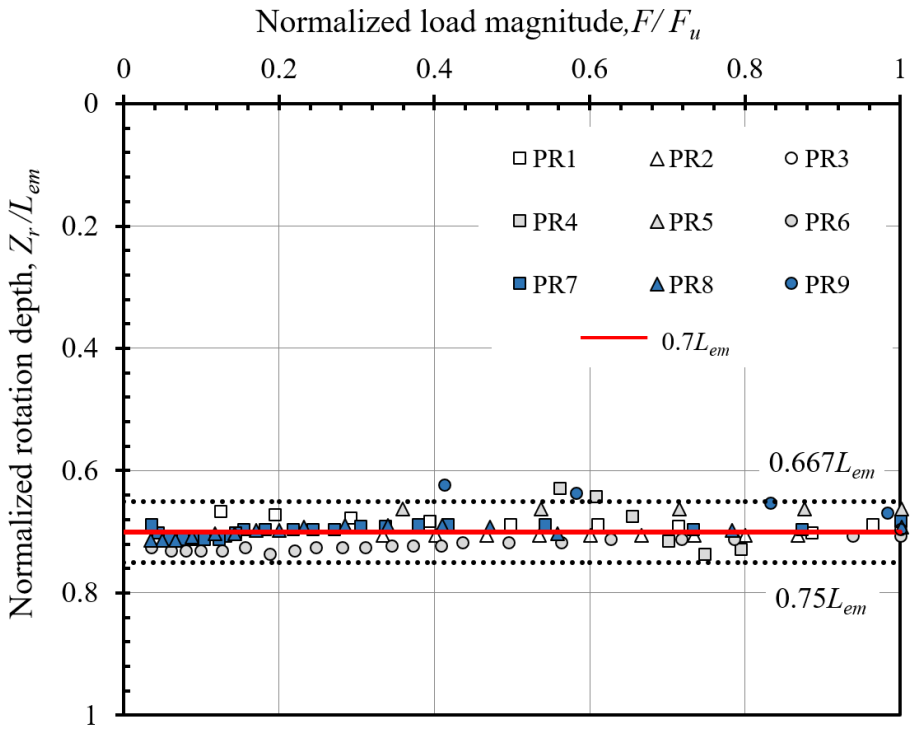


Figure 2. Variation of normalized rotation point depth for rigid pile in cohesive soil.

As shown in Figure 2, the normalized rotation depth Z_r/L_{em} is mainly located in the range of 0.65~0.75, and the depth of rotation point is approximately keeping constant irrespective of the dimension of monopile, soil condition, load eccentricity, and load levels. Based on the analysis above, the proposed design method in this paper assumes the depth of the rotation point (Z_r) is constant with the applied lateral load and equal to 0.70L_{em}. It should be noted that the assumed rotation point depth is consistent with the theoretical solution conducted by Darvishi-Alamouti et al. [34], in which the rotation point depth Z_r is in the range of 0.667~0.75L_{em} for rigid monopile in the soils with linearly varying modulus of subgrade reaction with depth.

2.2. Lateral Soil Reaction Profile

In the general design of laterally loaded monopiles in cohesive soil, the ultimate lateral resistance P_u of the ground soil is related to the undrained shear strength S_u with the lateral bearing factor N_p and pile outer diameter D:

$$P_u = N_p S_u D \quad (1)$$

A number of methods are available to determine the value of N_p, which were derived from experimental measurements, analytical solution, and engineering experience. Considering the different failure modes for the soil at shallow depths and deep depths, most of these methods define the value of N_p at ground surface and deep depths separately. The variations of N_p with depth from widely used methods are demonstrated in Figure 3. It can be seen from Figure 3 that the value of N_p is in the range of 2~4.83 at the ground surface and the limit value is in the range of 8~12.2 at deep depths. The critical depth for reaching the limit value of N_p is in the range of 1.5D~4D, and mostly at a depth of about 3D. In this study, the value of N_p at ground surface is assumed to be zero, and the depth to reach the limit value of N_p is 2D, as shown in Figure 3. Based on these two assumptions, i.e., a value of N_p = 0 at ground surface and a shallower critical depth (2D), the total soil lateral reaction in the depth of the upper 3D is comparable to that calculated by the existing methods (e.g., Reese et al. [8]; Randolph and Houlsby [35]).

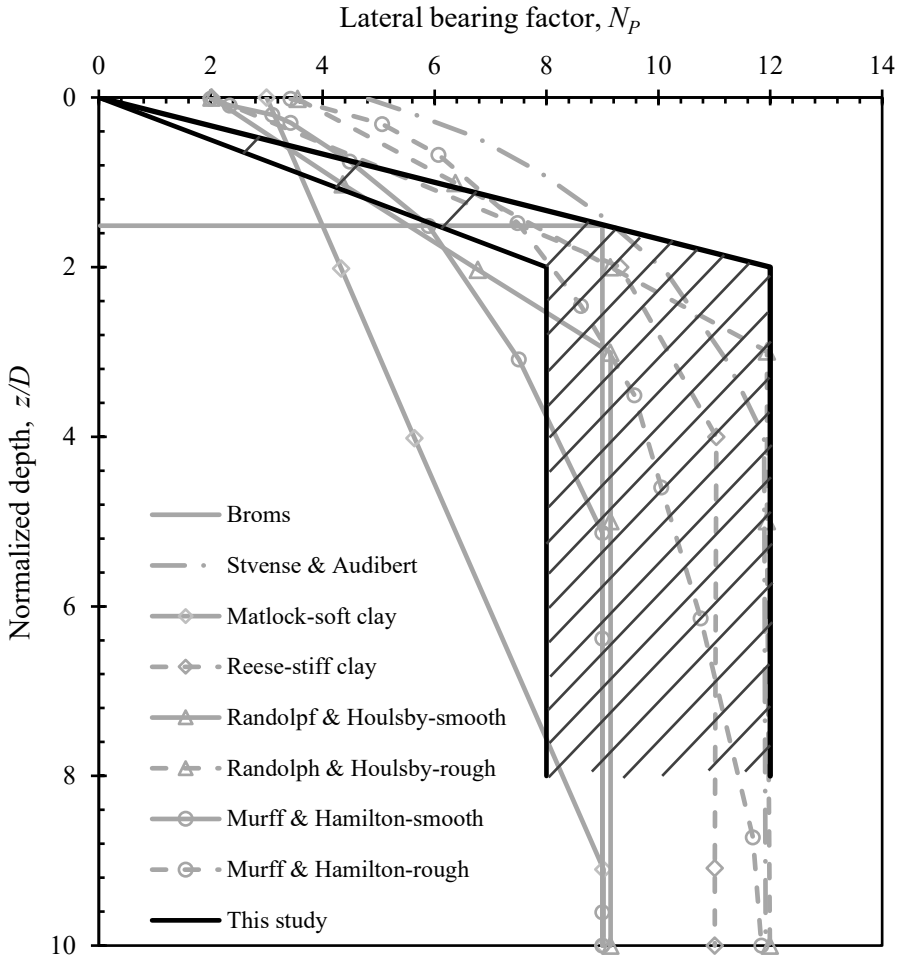


Figure 3. Variation of lateral bearing factor Np with normalized depth [7,8,35–38].

2.3. Mobilization Coefficient of Lateral Soil Reaction

Based on the depth of rotation point described in the previous section and the assumed variation of N_p with depth, this study-proposed profile of soil lateral reaction on the laterally loaded rigid monopile in cohesive soil is sketched in Figure 4, which may be described in the follow ways:

- At a given load level applied at the pile head, as the depth increasing, the magnitude of the soil lateral reaction generally increases linearly from zero at the ground surface to a depth of 2D; then, the soil reaction keeps as a constant in the depth range from 2D to Z_m, where Z_m is the maximum depth for the limit soil reaction. Following that,

the lateral soil reaction decreases linearly to zero at the depth of rotation point; at the rear side, the soil lateral reaction linearly increases from zero at the rotation point to a maximum value at the pile tip.

- The maximum soil reaction in the front side of monopile is p_m, which depends on the lateral undrained soil strength S_u and mobilization coefficient η of soil resistance. This coefficient is introduced to quantify the amount of soil resistance mobilized under a certain load level applied at the monopile head.
- Based on the equilibriums of lateral force and the moment of the monopile, Equation (2) is derived, and the correlation between applied lateral load and the mobilization coefficient η is established, see Equation (3).

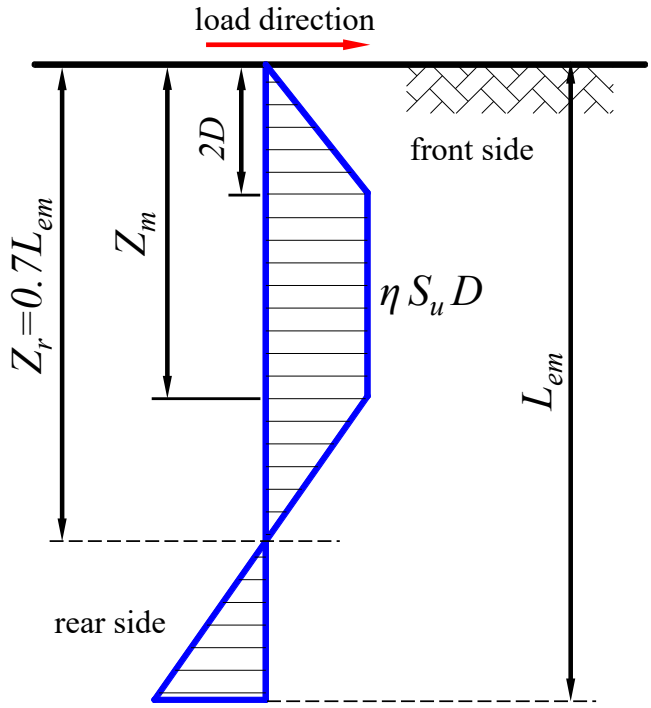


Figure 4. Assumed soil lateral reaction profile.

$$Z_m{}^3 + 3L_{up}Z_m{}^2 - D(4D + 6L_{up})Z_m + L_{em}D(2.8D + 4.2L_{up}) - 0.1L_{em}{}^3 - 1.2L_{em}{}^2L_{up} = 0 \quad (2)$$

$$\eta = \frac{F}{S_u D\left(0.35L_{em} - D + 0.5Z_m - \frac{0.045L_{em}{}^2}{0.7L_{em} - Z_m}\right)} \quad (3)$$

As shown in Equation (2), the depth of maximum soil reaction Z_m can be obtained conveniently by solving the equation. It is only related to the monopile embedded length L_{em}, pile diameter D, and load eccentricity L_{up}, and is independent of the magnitude of the applied lateral load F, which is in line with the observations by Zhang et al. [39] and Prasad and Chari [40].

It should be pointed out that as a critical depth of $2D$ and a rotation depth of $0.7L_{em}$ are assumed for the lateral soil reaction profile in this study, a minimum pile length L_{em} is existed to ensure that the calculated maximum depth for the limit soil reaction Z_m is not smaller than $2D$. Based on Equation (2), the minimum pile length L_{em} is derived, and the variation of minimum pile length with loading eccentricity is presented in Figure 5. As shown in Figure 5, the minimum pile length L_{min} is decreased nonlinearly from $5.3D$ to $3.6D$ with the increasing of loading eccentricity L_{up} from 0 to $15D$. The minimum pile length L_{min} decreased remarkably when the loading eccentricity is within $5D$, and beyond that, the minimum pile length L_{min} decreased slightly.

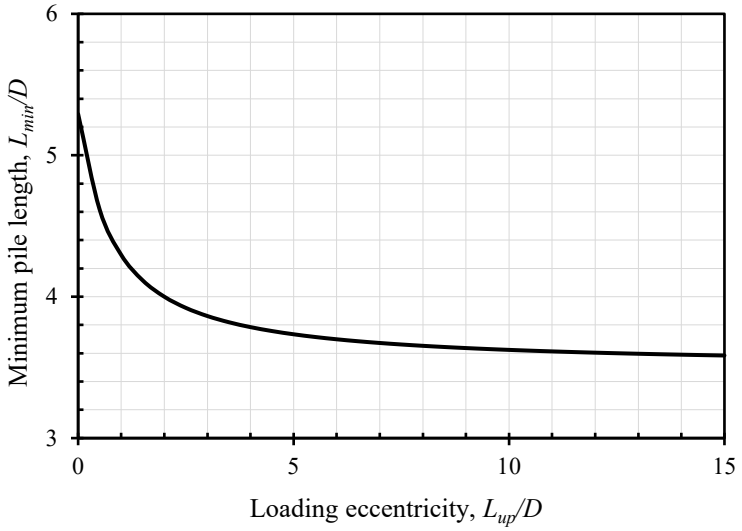


Figure 5. Variation of minimum pile length with loading eccentricity.

2.4. Correlation between Pile Rotation and Mobilization Coefficient

Since the amount of mobilized soil lateral resistance depends on the magnitude of applied load, a correlation between mobilization coefficient η and pile deformation (e.g., pile head rotation θ) should exist, and this correlation reflects the nonlinear response between soil and pile. To derive this correlation, pile response measured from a series of pile loading tests is employed. These test piles were installed in the cohesive soil with a wide range of dimensions and were loaded monotonically. The diameter of these test piles is up to 3.8 m in prototype, and the slenderness ratio L_{em}/D ranges from 4.8 to 11.8. The load eccentricity L_{up} is in the range of 0.2~7.89D. For the laterally loaded monopile, the larger the load eccentricity L_{up} is, the greater the bending moment act on the pile head for the same horizontal load. Therefore, it could be expected that increasing the load eccentricity will decrease the bearing capacity. However, as illustrated in Figure 2, the rotation depth Z_r is irrelevant to the load eccentricity L_{up}.

The soil condition involved in this database is from soft to stiff or over-consolidated clay, with an estimated undrained strength S_u ranging from 2.6 to 228 kPa. The soil rigidity factor K, defined as $K = E_s/S_u$, is estimated according to Equation (4) [22]:

$$K = \frac{E_s}{S_u} = \frac{2R_f}{\varepsilon_{50}(2R_f - 1)} \tag{4}$$

where:

E_s is soil elastic modulus; R_f is the soil failure ratio, with typical value of R_f = 0.75~1.0; and ε_{50} is the strain corresponding to one half of the maximum principal stress difference.

The soil rigidity factor is 200~500 in the collected database, which covers the range for the typical clay suggested by USACE [41]. Details of each pile test are summarized in Table 2. Case C1-1, C1-2, and C2 are centrifuge tests, which can produce data to improve our understanding of basic mechanisms of laterally loaded piles' deformation and failure.

Table 2. Details of laterally loaded pile tests.

Pile No.	Prototype Monopile Dimensions			Soil Condition			Pile Type	Site Location	Test Description	Reference
	D(m)	L_{em}/D	L_{up}/D	Description	S_u (kPa)	E_s/S_u				
F1	0.92	6.6	0.83	Stiff clay	100	250 *	Concrete pile	Texas A&M University	Field test	Kasch et al. [26]
F2-1	0.915	6.7	0.86	Stiff clay	100	250 *	Concrete pile	Texas A&M University	Field test	Bierschwale et al. [29]
F2-2	0.915	5								
F3-1	0.9	6.7								
F3-2	0.9	5	0.2	Stiff clay	100	250 *	Concrete pile	Texas A&M University	Field test	Briaud et al. [42]
F3-3	0.75	6								
F4	0.61	7.75	0.38	sandy clay	228	347 **	Concrete pile	Los Angeles, USA	Field test	Bhushan et al. [43]
F5	0.92	5	0.87	Stiff clay	110	250 *	Concrete pile	Texas A&M University	Field test	Holloway et al. [27]
F6	0.51	4.8	0.5	medium stiff clay	60	-	Concrete pile	University of Massachusetts Amherst	Field test	Lutenegger and Miller [44]
F7-1	0.762	4.8	4	Stiff clay	155	450 **	Concrete pile	Colorado, USA	Field test	Nusairat et al. [45]
F7-2	0.762	4.8	1		100	375 **	Concrete pile		Field test	
M1-1	0.089	8	0.22	Over-consolidated kaolin clay	7	200	Concrete pile	-	Model test	Mayne et al. [46]
M1-2	0.089	6			6					
M2-1	0.089	8	0.22	Over-consolidated kaolin clay	5.7	200	Concrete pile	-	Model test	Mayne et al. [47]
M2-2	0.089	6	0.22		5.4					
M2-3	0.089	6	24		2.6					
C1-1	0.88	11.8	0.15	kaolin clay	8.5	400	Aluminum pipe pile	University of Western Australia	centrifuge test	Guo et al. [48]
C1-2	0.44	11.8			6.6					
C2	3.8	5.26	7.89	over-consolidated Kaolin clay	18	500 †	Aluminum pipe pile	University of Cambridge	centrifuge test	Lau et al. [31]

* obtained from Zhang and Ahmari [22]; ** obtained from Equation (4); † obtained from Haiderali et al. [49].

To derive the correlation between mobilization coefficient η and pile head rotation θ from measured response of each pile test, three steps are followed.

1. For a specifically applied lateral load F_i, the mobilization coefficient η_i is calculated with Equations (2) and (3);
2. The pile head rotation θ_i or displacement y_i corresponding to this applied load F_i can be read from the measured pile head response. If only y_i is measured, the corresponding pile head rotation θ_i can be calculated with Equation (5), see Figure 6;

$$\theta_{\mathrm{i}} = \arctan\left(\frac{y_i}{h + 0.7L_{em}}\right) \tag{5}$$

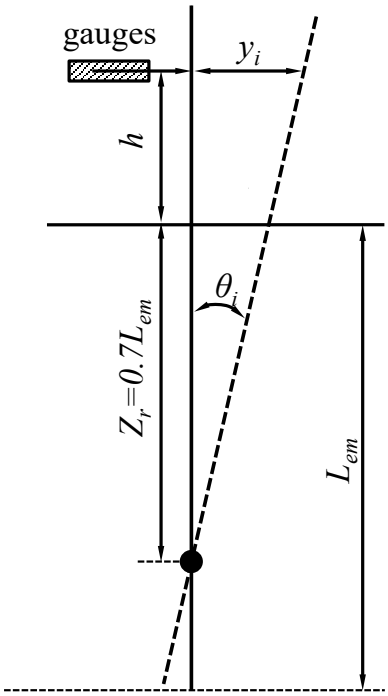


Figure 6. Sketch of pile rotation.

For another load level, by repeating these steps, the correlation between η and θ is derived for each pile, which is shown in Figure 7. As expected, the back-calculated mobilization coefficient of soil resistance increases nonlinearly with the increasing of monopile rotation. In addition, the relationship between the mobilization coefficient and pile rotation may be approached by a hyperbolic function, as illustrated in Figure 7. Therefore, the hyperbolic function proposed by Duncan et al. [50] is adopted, see Equation (6):

$$\eta = \frac{\theta}{\frac{1}{K_{ini}} + R_f \frac{\theta}{\eta_{max}}} \tag{6}$$

where:

K_{ini} = initial stiffness of the η-θ curve;
R_f = soil failure ratio, and ranging from 0.75 to 0.95 recommended by Duncan et al. [50];
η_{max} = maximum mobilization coefficient.

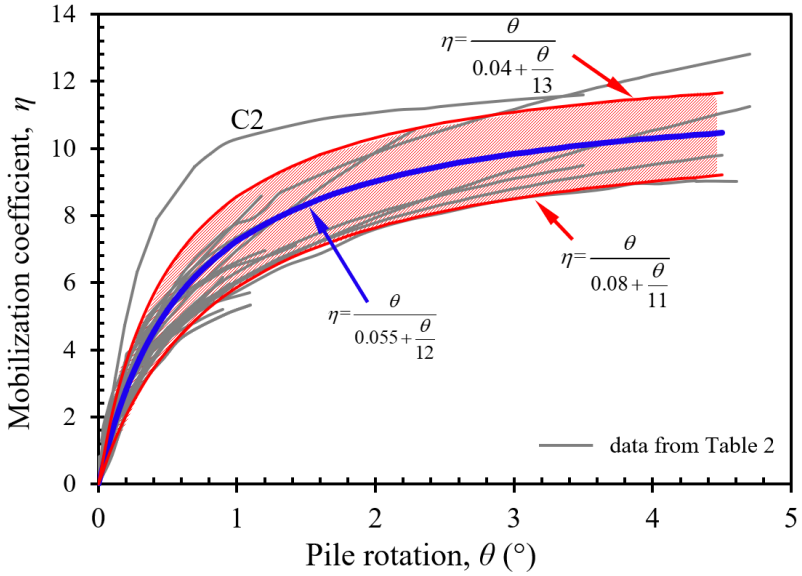
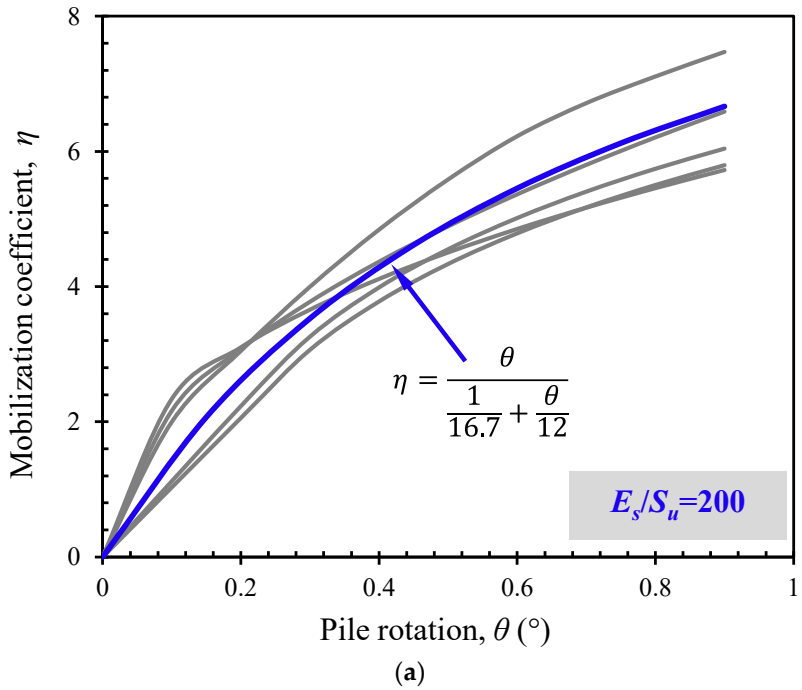


Figure 7. Correlation between monopile rotation and mobilization coefficient of soil resistance.

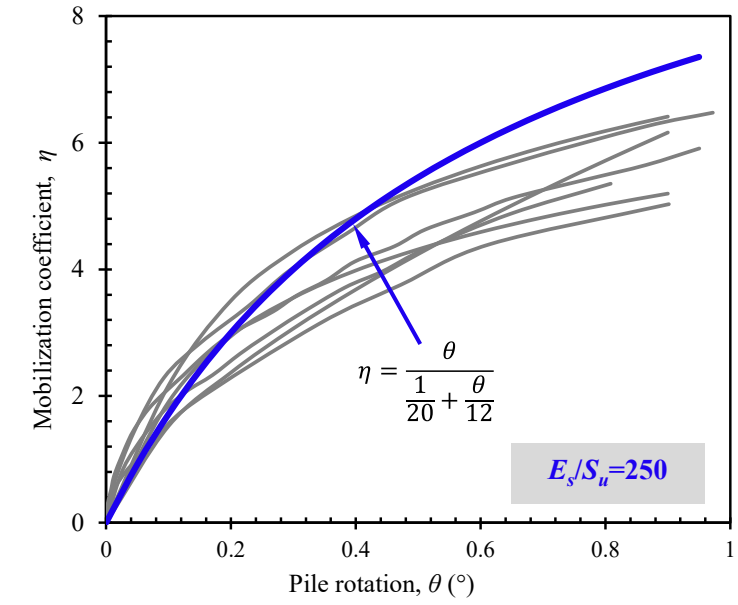
Based on the fitted correlations between the mobilization coefficient and pile rotation, the values of η_{max} mainly range from 9.9~11.7 (assumes that R_f = 0.9), which agree with the limit value of N_p as illustrated in Figure 3.

In order to estimate the value of K_{ini} in Equation (6), the derived value of K_{ini} is plotted with soil rigidity factor K (=E_s/S_u) for each pile test, see Figure 8. For simplicity and to reduce the effect of maximum mobilization coefficient η_{max} and soil failure ratio R_f, a constant value of 12 is set for the ratio of η_{max} to R_f.

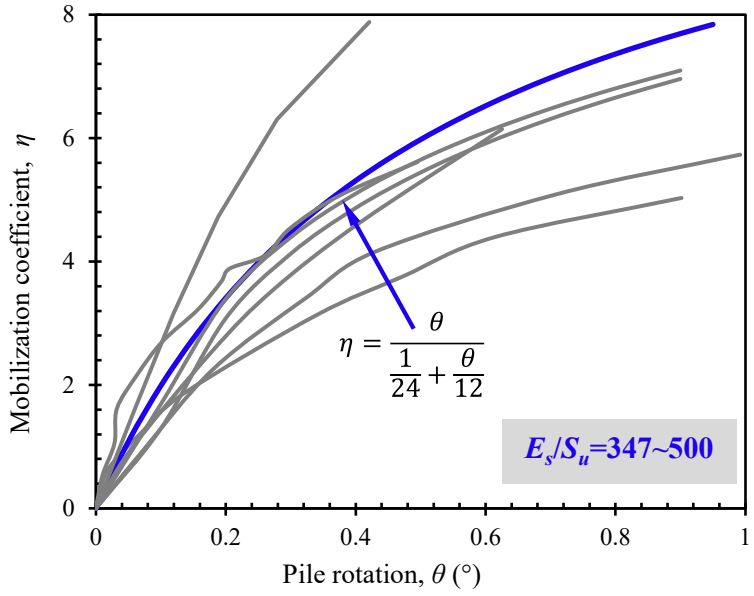


(**a**)

Figure 8. *Cont.*



(**b**)



(**c**)

Figure 8. Correlations between pile rotation and mobilization coefficient for various ground conditions: (**a**) E_s/S_u = 200; (**b**) E_s/S_u = 250; (**c**) E_s/S_u = 347~500.

Figure 8 shows that the hyperbolic function simulates the variation of the mobilization coefficient with pile rotation successfully for various ground conditions, and the value of initial stiffness K_{ini} in Equation (6) increases as the increasing of the soil rigidity. To construct a correlation between the initial stiffness K_{ini} and soil rigidity factor K, the values of K_{ini} are plotted with soil rigidity factors K for each group of pile tests, see Figure 9, which demonstrates that a linear function (K_i = 0.04K + 10.2) fits the variation of initial stiffness with the soil rigidity factor well. It should be noted that the soil rigidity studied in this study ranges from 200 to 500, see Table 2.

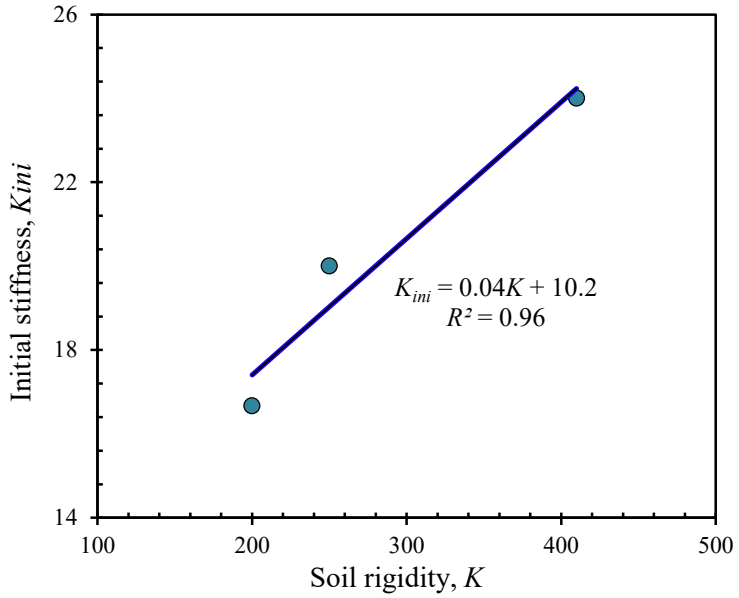


Figure 9. Variation of initial stiffness Kini with soil rigidity *K*.

3. Validation of the Proposed Design

3.1. General Design Procedures

To design a laterally loaded rigid monopile in cohesive soil, the following procedure is recommended by this study:

1. According to the ground soil condition, the soil rigidity E_s/S_u is estimated and the value of K_{ini} can be determined according to Equation (7), see Figure 9;

$$K_{ini} = 0.04 \cdot \frac{E_s}{S_u} + 10.2 \tag{7}$$

2. Set a specific value of pile head rotation θ_i or pile displacement y_i; the mobilization coefficient η_i can be determined according to Equations (6) and (7). Based on Figure 7, the average value of $\eta_{max}/R_f = 12$ is recommended in this study. Thus, the mobilization coefficient η_i can be calculated as following:

$$\eta_i = \frac{\theta_i}{\frac{1}{K_{ini}} + \frac{\theta_i}{12}} \tag{8}$$

3. Calculate the corresponding pile head load F_i with Equation (9), as well as the pile displacement with Equation (10);

$$F_i = \eta_i S_u D(0.35L_{em} - D + 0.5Z_m - \frac{0.045{L_{em}}^2}{0.7L_{em} - Z_m}) \tag{9}$$

$$y_i = \tan\theta_i \cdot (h + 0.70L_{em}) \tag{10}$$

4. Repeating steps 1 to 3, the general pile response of monopile is estimated under various magnitudes of applied lateral loads.

3.2. Verification

To verify the feasibility and reliability of this study proposed design, three numerical simulations including 5 cases are collected in this section, and the load-displacement responses calculated with this study-proposed method are compared with those by numerical simulation.

3.2.1. Case 1

In order to verify the proposed design method, two laterally loaded monopiles in cohesive soil simulated by Georgiadis and Georgiadis [51] are employed. The uniform undrained soil strength S_u is 70 kPa, and the initial elasticity modulus is E_s = 23.38 MPa. The detailed dimensions of the two monopiles and soil conditions are presented in Table 3.

Table 3. Parameters of monopiles and soil condition for case 1.

Pile No.	D(m)	L_{em}/D	L_{up}/D	S_u(kPa)	E_s/S_u
I	1	5	0	70	334
II	1	10	0	70	334

Based on Equation (7), the correlation between mobilization coefficient η and pile rotation θ is adopted as following:

$$\eta = \frac{\theta}{0.042 + \frac{\theta}{12}} \tag{11}$$

Figure 10 shows the comparisons of pile-head load displacements between the numerical simulation and prediction within this study-proposed method. It demonstrates a good agreement and proves the validity of the proposed method in the lateral deformation prediction of laterally loaded monopile. It should be noted that although the pile length L_{em} is a little smaller than the minimum pile length L_{min} for pile I, in which the calculated Z_m is about 1.8D, the proposed design method is still suitable according to the comparisons.

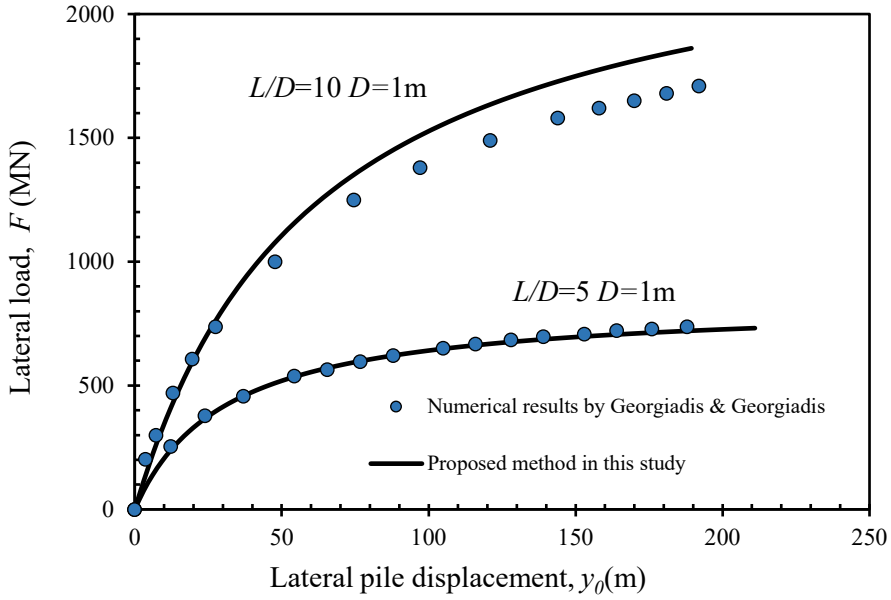


Figure 10. Comparisons of the load displacement results for case 1 [51].

3.2.2. Case 2

Another numerical case conducted by Zhang et al. [22] is employed to verify the proposed design method. The diameter of simulated lateral loaded pile is 1 m, with a slenderness ratio L_{em}/D = 5 and load eccentricity ratio L_{up}/D = 1. The simulated soil material is stiff clay with undrained strength S_u = 100 kPa and stiffness ratio E_s/S_u = 250.

The correlation between the mobilization coefficient η and pile rotation θ is adopted as the following:

$$\eta = \frac{\theta}{0.05 + \frac{\theta}{12}} \tag{12}$$

As shown in Figure 11, the proposed design method agrees well with the numerical pile head response, which demonstrates the validity of the proposed design method. In addition, analytical prediction given by Zhang et al. [22] is also shown in Figure 11, and the proposed method in this paper agrees better than Zhang's method in general. Besides, the parameters used in the proposed method in this paper are easier to determine, so it is more convenient to employe in practical engineering designs.

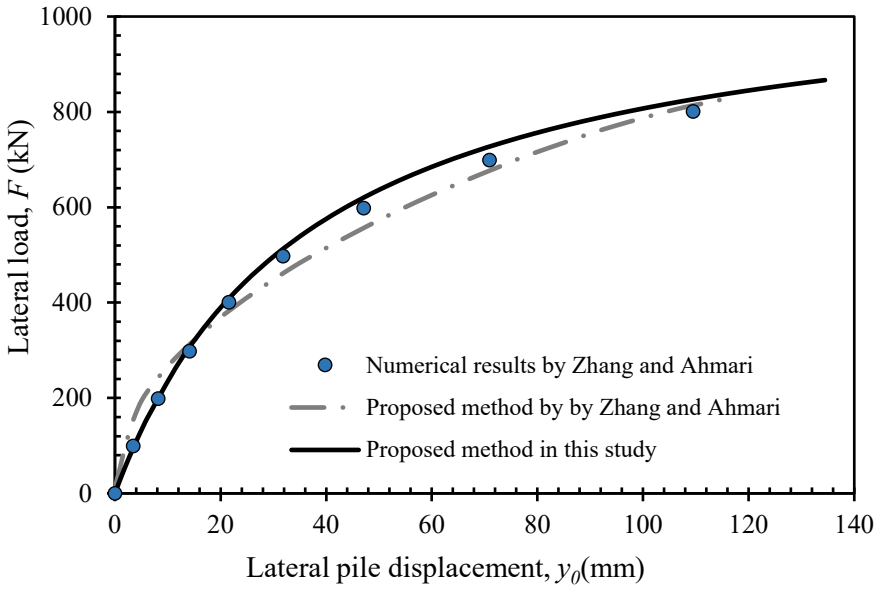


Figure 11. Comparison of the load displacement results for case 2 [22].

3.2.3. Case 3

To investigate the feasibility of the proposed design method for large diameter monopiles used in offshore wind turbines, two large diameter monopiles embedded in stiff glacial clay till deposits simulated by Zdravkovic et al. [33] via advanced numerical program are employed. The undrained soil strength S_u in this site is generally increased linearly with depth, and the representative soil strength S_u is determined according to the soil strength profile with a reference depth of $L_{em}/2$ in this paper. According to Powell and Butcher [52], the shear modulus G_s at a depth of $L_{em}/2$ in this site is about 18 MPa and, thus, a elasticity modulus $E_s = 18 \times 2 \times (1 + 0.5) = 54$ MPa under undrained condition can be obtained. The detailed pile dimensions of the two monopiles and soil conditions are presented in Table 4.

Table 4. Parameters of monopiles and soil condition for case 3.

Pile No.	D(m)	L_{em}/D	L_{up}/D	S_u(kPa)	E_s/S_u
I	10	6	5	180	300
II	10	6	15	180	300

According to Equation (7), the correlation between mobilization coefficient η and pile rotation θ is adopted as following:

$$\eta = \frac{\theta}{0.045 + \frac{\theta}{12}} \tag{13}$$

Comparisons of pile-head load displacement behaviors predicted by numerical simulation and the proposed method in this paper are plotted in Figure 12, which shows a good agreement and proves the validity of the proposed method in the lateral deformation

prediction of large diameter monopile in the site with undrained soil strength increased with depth.

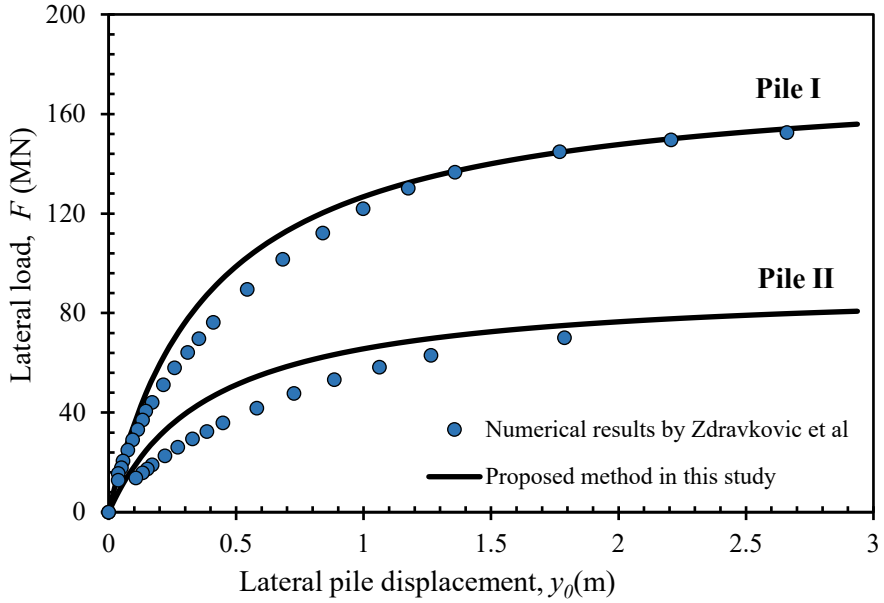


Figure 12. Comparison of monopile head load displacement response for case 3 [33].

4. Conclusions

A static design for laterally loaded rigid monopiles in cohesive soil is presented in this study. This method is verified against three numerical cases including five pile tests, and the results show that this method produces a reasonably good prediction of response for rigid monopiles embedded in the sites with undrained shear strength being uniform or increasing linearly with depth. This method not only takes account for the nonlinear interaction between monopiles and around soil, but also can be applied without computer programming, which is very convenient for the preliminary design of an industrial project. The main findings are as following:

- The normalized rotation depth Z_r/L_{em} is mainly located in the range of 0.65~0.75 for rigid monopile embedded in cohesive soil, which keeps approximately as a constant regardless of the dimensions of monopile, soil condition, load eccentricity, and load levels. In this study a rotation depth of $0.7L_{em}$ is assumed to derive a simple design for laterally loaded monopiles in cohesive soil.
- A mobilization coefficient of soil resistance η is introduced to quantify the magnitude of soil resistance mobilized under various lateral displacements of monopiles, and the correlation between coefficient η and monopile rotation θ is constructed by back-analyzing-measured results from a series of test piles reported in the literature. It shows that the relationship between coefficient η and pile head rotation θ can be well approached by a hyperbolic function.
- The values of η_{max} in the hyperbolic function mainly ranges from 9.9 to 11.7, and a linear function is adopted to simulate the variation of initial stiffness K_{ini} with soil rigidity factor K for ground soils with rigidity ranging from 200 to 500, in which $K_{ini} = 0.04K + 10.2$.
- It should be noted that a minimum pile length L_{em} existed to satisfy the proposed lateral soil reaction profile, and the minimum pile length L_{min} is decreased nonlinearly from $5.3D$ to $3.6D$ with the increasing of loading eccentricity L_{up} from 0 to $15D$.
- The load-displacement responses analyzed by the proposed method are compared with the numerical results published in the literature to validate the reliability of the proposed method, which show that it can be used well for laterally loaded monopile

design in the sites with undrained shear strength being uniform or increasing linearly with depth.

It should be noted that, considering the nature of the offshore environmental loading condition, cyclic/dynamic loading is predominant for the monopile used in OWTs, and it is not considered in this study.

Author Contributions: Conceptualization, R.L. and W.L.; methodology, R.L. and M.H.; validation, M.H. and A.W.; formal analysis, M.H. and A.W.; investigation, R.L.; writing—original draft preparation, R.L.; writing review and editing, R.L. and W.L.; visualization, R.L. and W.L.; supervision, M.Y. and W.L.; funding acquisition, L.R, W.L. and A.W. All authors have read and agreed to the published version of the manuscript.

Funding: This research was funded by National Natural Science Foundation of China (Grant No. 52208343, 41877236, 41972275 and 52020105003), Natural Science Foundation of Jiangsu Province of China (BK20210051) and Key Laboratory of Ministry of Education for Geomechanics and Embankment Engineering, Hohai University (No. 2021001).

Institutional Review Board Statement: Not applicable.

Informed Consent Statement: Not applicable.

Data Availability Statement: Not applicable.

Acknowledgments: The authors acknowledge the funding received from National Natural Science Foundation of China, Natural Science Foundation of Jiangsu Province of China and Key Laboratory of Ministry of Education for Geomechanics and Embankment Engineering, Hohai University for supporting this research.

Conflicts of Interest: The authors declare no conflict of interest.

Notation

D	outer diameter of monopile
E_s	soil elastic modulus
E_p	elastic modulus of pile
F	lateral load acted on monopile head
F_u	pile ultimate load capacity
h	height of displacement measured
I_p	inertia moment of pile
K	soil rigidity factor
K_i	initial stiffness of the η-θ curve
L_{em}	embedded length of monopile
L_{min}	minimum pile length
L_{up}	load height above ground level
M	moment applied on monopile head
n_h	constant of horizontal subgrade reaction
N_p	lateral limit bearing factor
P	lateral soil reaction
P_u	ultimate soil lateral resistance
p_m	maximum soil reaction in the front side of monopile
R_f	soil failure ratio
S_u	soil undrained shear strength
y_0	lateral displacement of rigid monopile
Z_m	depth of maximum soil lateral reaction
Z_r	depth of rotation point
θ	rotation of monopile
η	mobilization coefficient of soil lateral resistance
η_{max}	maximum mobilization coefficient
Q_b	normalized load magnitude

References

1. Yang, M.; Luo, R.; Li, W. Numerical study on accumulated deformation of laterally loaded monopiles used by offshore wind turbine. *Bull. Eng. Geol. Environ.* **2018**, *77*, 911–921. [CrossRef]
2. Luo, R.; Zhu, B.; Yang, Z. Limiting force profile for laterally loaded piles in undrained clay. *Int. J. Geomech.* **2021**, *21*, 04021146. [CrossRef]
3. Lai, Y.; Wang, L.; Hong, Y.; He, B. Centrifuge modeling of the cyclic lateral behavior of large-diameter monopiles in soft clay: Effects of episodic cycling and reconsolidation. *Ocean. Eng.* **2020**, *200*, 107048. [CrossRef]
4. LeBlanc, C.; Houlsby, G.T.; Byrne, B.W. Response of stiff piles in sand to long-term cyclic lateral loading. *Geotechnique* **2010**, *60*, 79–90. [CrossRef]
5. Ahmed, S.S.; Hawlader, B. Numerical analysis of large-diameter monopiles in dense sand supporting offshore wind turbines. *Int. J. Geomech.* **2016**, *16*, 04016018. [CrossRef]
6. Luo, R.; Yang, M.; Li, W. Numerical study of diameter effect on accumulated deformation of laterally loaded monopiles in sand. *Eur. J. Environ. Civ. Eng.* **2020**, *24*, 2440–2452. [CrossRef]
7. Matlock, H. Correlations for design of laterally loaded piles in soft clay. In Proceedings of the 2nd Annual Offshore Technology Conference, Houston, TX, USA, 22–24 April 1970; Volume 1, pp. 577–594.
8. Reese, L.C.; Cox, W.P.; Koop, F.D. Field testing and analysis of laterally loaded piles in stiff clay. In Proceedings of the 7th Offshore Technology Conference, Houston, TX, USA, 5–8 May 1975; Volume 2, pp. 671–690.
9. Kim, B.T.; Kim, N.K.; Lee, W.J.; Kim, Y.S. Experimental load–transfer curves of laterally loaded piles in Nak-Dong River sand. *J. Geotech. Geoenviron. Eng.* **2004**, *130*, 416–425.
10. Byrne, B.W.; Houlsby, G.T.; Burd, H.J.; Gavin, K.G.; Igoe, D.J.; Jardine, R.J.; Martin, C.M.; McAdam, R.A.; Potts, D.M.; Taborda, D.M.G.; et al. PISA design model for monopiles for offshore wind turbines: Application to a stiff glacial clay till. *Géotechnique* **2020**, *70*, 1030–1047. [CrossRef]
11. Wang, L.; Lai, Y.; Hong, Y.; Mašín, D. A unified lateral soil reaction model for monopiles in soft clay considering various length-to-diameter (L/D) ratios. *Ocean Eng.* **2020**, *212*, 107492. [CrossRef]
12. Cao, G.; Ding, X.; Yin, Z.; Zhou, H.; Zhou, P. A new soil reaction model for large-diameter monopiles in clay. *Comput. Geotech.* **2021**, *137*, 104311. [CrossRef]
13. Munaga, T.; Gonavaram, K.K. Influence of stratified soil system on behavior of laterally loaded pile groups: An experimental study. *Int. J. Geosynth. Ground Eng.* **2021**, *7*, 18. [CrossRef]
14. Rathod, D.; Nigitha, D.; Krishnanunni, K.T. Experimental investigation of the behavior of monopile under asymmetric two-way cyclic lateral loads. *Int. J. Geomech.* **2021**, *21*, 06021001. [CrossRef]
15. Yu, F.; Zhang, C.; Huang, M.; Yang, X.; Yao, Z. Model Tests on Cyclic Responses of a Laterally Loaded Pile Considering Sand Anisotropy and Scouring. *J. Mar. Sci. Eng.* **2023**, *11*, 255. [CrossRef]
16. Kozubal, J.; Puła, W.; Wyjadłowski, M.; Bauer, J. Influence of varying soil properties on evaluation of pile reliability under lateral loads. *J. Civ. Eng. Manag.* **2013**, *19*, 272–284. [CrossRef]
17. Li, B.; Wang, Y.; Qi, W.; Wang, S.; Gao, F. Lateral Bearing Capacity of a Hybrid Monopile: Combined Effects of Wing Configuration and Local Scour. *J. Mar. Sci. Eng.* **2022**, *10*, 1799. [CrossRef]
18. Wang, H.; Wang, L.; Hong, Y.; Askarinejad, A.; He, B.; Pan, H. Influence of Pile Diameter and Aspect Ratio on the Lateral Response of Monopiles in Sand with Different Relative Densities. *J. Mar. Sci. Eng.* **2021**, *9*, 618. [CrossRef]
19. Huchegowda, B.K.; Teja, M.; Kalyan Kumar, G. Evaluation of lateral capacity of pile foundation using finite Element method in layered soil. In *Advances in Geotechnical and Transportation Engineering: Select Proceedings of FACE*; Springer: Singapore, 2020; pp. 79–84.
20. Zhang, L. Nonlinear analysis of laterally loaded rigid piles in cohesionless soil. *Comput. Geotech.* **2009**, *36*, 718–724. [CrossRef]
21. Motta, E. Lateral deflection of horizontally loaded rigid piles in elastoplastic medium. *J. Geotech. Geoenviron. Eng.* **2013**, *139*, 501–506. [CrossRef]
22. Zhang, L.; Ahmari, S. Nonlinear analysis of laterally loaded rigid piles in cohesive soil. *Int. J. Numer. Anal. Methods Geomech.* **2013**, *37*, 201–220. [CrossRef]
23. Fu, D.; Zhang, Y.; Aamodt, K.K.; Yan, Y. A multi-spring model for monopile analysis in soft clays. *Mar. Struct.* **2020**, *72*, 102768. [CrossRef]
24. Tomlinson, M.; Woodward, J. *Pile Design and Construction Practice*; Taylor & Francis: London, UK; New York, NY, USA, 2015.
25. Klinkvort, R.T.; Black, J.A.; Bayton, S.M.; Haigh, S.K.; Madabhushi, G.S.P.; Blanc, M.; Thorel, L.; Zania, V.; Bienen, B.; Gaudin, C. *A Review of Modelling Effects in Centrifuge Monopile Testing in Sand*; Taylor & Francis Group: Abingdon, UK, 2018; pp. 720–723.
26. Kasch, V.R.; Coyle, H.M.; Bartoskewitz, R.E.; Sarver, W.G. *Lateral Load Test of a Drilled Shaft in Clay; Research Report 211-1*; Texas Transportation Institute; The Texas A&M University System: College Station, TX, USA, 1977.
27. Holloway, G.L.; Coyle, H.M.; Bartoskewitz, R.E.; Sarver, W.G. *Field Test and Preliminary Design Method for Laterally Loaded Drilled Shafts in Clay; Rep. No. FHWATX78-211-2*; Texas Transportation Institute: College Station, TX, USA, 1978.
28. Ismael, N.F.; Klym, T.W. Behaviour of Rigid Piers in Layered Cohesive Soils. *J. Geotech. Eng.* **1978**, *104*, 1061–1074.
29. Bierschwale, M.W.; Coyle, H.M.; Bartoskewitz, R.E. Lateral load tests on drilled shafts founded in clay. In *Drilled Piers and Caissons*; ASCE: Reston, Virginia, 1981; pp. 98–113.

30. Pender, M.; Rodgers, P. Numerical modelling of lateral load-deformation curves for timber polesembedded in stiff clay. In Proceedings of the 19th International Conference on Soil Mechanics and Geotechnical Engineering, Seoul, Republic of Korea, 17–22 September 2017.
31. Lau, B.H.; Lam, S.Y.; Haigh, S.K.; Madabhushi, S.P.G. Centrifuge testing of monopile in clay under monotonic loads. In Proceedings of the 8th International Conference on Physical Modelling in Geotechnic, Perth, Australia, 14–17 January 2014; Volume 2, pp. 689–695.
32. Senanayake, A.I.M.J. Design of Large Diameter Monopiles for Offshore Wind Turbines in Clay. Ph.D. Thesis, The University of Texas at Austin, Austin, TX, USA, 2016.
33. Zdravković, L.; Taborda, D.M.G.; Potts, D.M.; Jardine, R.J.; Sideri, M.; Schroeder, F.C.; Byrne, B.W.; McAdam, R.; Burd, H.J.; Houlsby, G.T.; et al. Numerical modelling of large diameter piles under lateral loading for offshore wind applications. In Proceedings of the 3rd International Symposium on Frontiers in Offshore Geotechnics, Oslo, Norway, 10–12 June 2015.
34. Darvishi-Alamouti, S.; Bahaari, M.R.; Moradi, M. Natural frequency of offshore wind turbines on rigid and flexible monopiles in cohesionless soils with linear stiffness distribution. *Appl. Ocean Res.* **2017**, *68*, 91–102. [CrossRef]
35. Randolph, M.F.; Houlsby, G.T. Limiting pressure on a circular pile loaded laterally in cohesive Soil. *Géotechnique* **1984**, *34*, 613–623. [CrossRef]
36. Broms, B.B. Lateral resistance of piles in cohesive soils. *J. Soil Mech. Found. Div.* **1964**, *90*, 27–64. [CrossRef]
37. Stevens, J.B.; Audibert, J.M.E. Re-examination of p–y curves formulations. In Proceedings of the 11th Offshore Technology Conference, Houston, TX, USA, 30 April–3 May 1979; pp. 397–401.
38. Murff, J.D.; Hamilton, J.M. P-ultimate for undrained analysis of laterally loaded piles. *J. Geotech. Geoenviron ASCE* **1993**, *119*, 91–107. [CrossRef]
39. Zhang, L.; Silva, F.; Grismala, R. Ultimate lateral resistance to piles in cohesionless soils. *J. Geotech. Geoenviron. Eng.* **2005**, *131*, 78–83. [CrossRef]
40. Prasad, Y.; Chari, T. Lateral capacity of model rigid piles in cohesionless soils. *Soils Found.* **1999**, *39*, 21–29. [CrossRef]
41. U.S. Army Corps of Engineers (USACE). *Engineering and Design Settlement Analyses; Manual*; USACE: Washington, DC, USA, 1990; p. 150, No. 1110-1-1904.
42. Briaud, J.L.; Smith, T.D.; Meyer, B.J. Pressuremeter gives elementary model for laterally loaded piles. *Proa Int. Sym.-Situ Test. Soil Rock Paris* **1983**, *2*, 217–221.
43. Bhushan, K.; Haley, S.C.; Fong, P.T. Lateral load tests on drilled piers in stiff clays. *J. Geotech. Eng.* **1979**, *105*, 969–985. [CrossRef]
44. Lutenegger, A.J.; Miller, G.A. Behavior of Laterally Loaded Drilled Shafs in Stiff Soil. *Int. Conf. Case Hist. Geotech. Eng.* **1993**, *1*, 147–152.
45. Nusairat, J.; Liang, R.Y.; Engel, R.; Hanneman, D.; Abu-Hajleh, N.; Yang, K. *Drilled Shaft Design for Sound Barrier Walls, Signs and Signals*; Report no. CDOT-DTD-R-2004-8; Colorado Department of Transportation: Denver, CO, USA, 2004.
46. Mayne, P.W.; Kulhawy, F.H.; Trautmann, C.H. Laboratory modeling of laterally-loaded drilled shafts in clay. *J. Geotech. Eng.* **1995**, *121*, 827–835. [CrossRef]
47. Mayne, P.W.; Kulhawy, F.H.; Trautmann, C.H.; Kulhawy, F.H. *Experimental Study of Undrained Lateral and Moment Behavior of Drilled Shafts during Static and Cyclic Loading*; No., EPRI-TR-100221; Electric Power Research Institute: Palo Alto, CA, USA; Cornell University: Ithaca, NY, USA; Geotechnical Engineering Group: Las Vegas, NV, USA, 1992.
48. Guo, F.; Lehane, B.M.; Ju, J. Experimentally derived CPT-based p-y curves for soft clay. In Proceedings of the 3rd International Symposium on Cone Penetration Testing, Las Vegas, NV, USA, 13–14 May 2014; pp. 1021–1028.
49. Haiderali, A.E.; Nakashima, M.; Madabhushi, S.P.G. Cyclic lateral loading of monopiles for offshore wind turbines. In *Frontiers in Offshore Geotechnics III, Proceedings of the 3rd International Symposium on Frontiers in Offshore Geotechnics (ISFOG 2015), Oslo, Norway, 10–12 June 2015*; Taylor & Francis Books Ltd.: Abingdon, UK, 2015; Volume 1, pp. 711–716.
50. Duncan, J.M.; Evans, L.T., Jr.; Ooi, P.S. Lateral load analysis of single piles and drilled shafts. *J. Geotech. Eng.* **1994**, *120*, 1018–1033. [CrossRef]
51. Georgiadis, K.; Georgiadis, M. Undrained lateral pile response in sloping ground. *J. Geotech. Geoenviron. Eng.* **2010**, *136*, 1489–1500. [CrossRef]
52. Powell, J.J.M.; Butcher, A.P. Characterisation of a glacial clay till at Cowden, Humberside. *Charact. Eng. Prop. Nat. Soils* **2003**, *2*, 983–1020.

Disclaimer/Publisher's Note: The statements, opinions and data contained in all publications are solely those of the individual author(s) and contributor(s) and not of MDPI and/or the editor(s). MDPI and/or the editor(s) disclaim responsibility for any injury to people or property resulting from any ideas, methods, instructions or products referred to in the content.